Eur. Phys. J. D **27**, 223–229 (2003)
DOI: 10.1140/epjd/e2003-00268-4

THE EUROPEAN PHYSICAL JOURNAL D

Model analysis of the fragmentation of large H_2O and NH_3 clusters based on MD simulations

T.A. Beu[1], C. Steinbach[2], and U. Buck[2,a]

[1] University "Babeş-Bolyai", Faculty of Physics, 3400 Cluj-Napoca, Romania
[2] Max–Planck–Institut für Strömungsforschung, Bunsenstraße 10, 37073 Göttingen, Germany

Received 27 March 2003 / Received in final form 25 June 2003
Published online 26 August 2003 –

Abstract. The fragmentation statistics of $(H_2O)_n$ and $(NH_3)_n$ clusters ($n = 100$–1000) is investigated by MD simulations at different temperatures. The fragment size distributions are found to be well described by power laws over a wide range of excitation energies. The maximum fragment size depends linearly on the cluster size. A compact analytical model, implying the maximum fragment size and the power law exponent, is shown to fairly fit the average fragment size profiles. Measurements are carried out for the maximum fragment sizes after electron impact ionisation for water and ammonia clusters in the size range of $n = 50$ to 2100. The measured linear dependence on cluster size is used to estimate the fragment size distributions.

PACS. 36.40.-c Atomic and molecular clusters – 36.40.Qv Stability and fragmentation of clusters

1 Introduction

Fragmentation of particles is a widespread phenomenon, which occurs in large molecules, atomic and molecular clusters, as well as in nuclei after the interaction of the particles with photons or other particles. This ubiquitous behaviour has evoked the search for an universal mechanism that governs all these processes. This is, however, a difficult task, since many of the available data are incomplete and are therefore difficult to compare. In addition, there are many theoretical approaches accessible which reach from pure statistical considerations with and without thermodynamical constraints over percolation theory to Molecular Dynamics (MD) simulations which take into account the realistic interaction forces and contain all couplings. The success or failure of the different theoretical descriptions depends largely on the type of data sets. There are mainly three different fragmentation regimes. At low excitation energies mainly large and small fragments result. This is the "evaporation" regime where a small number of single particles evaporates and the size dependence is exponential [1]. At high excitation energies, the original particle falls completely into small pieces and this is "the shattering" regime [2]. Sometimes, an intermediate case occurs where the distribution of fragments follows a power law. This latter case can be nicely described by percolation theory, in which the ansatz $P_n(s) \sim s^{-\phi} G(s/n)$ is used for the formation probability of a fragment of size s coming from a cluster of size n [1,3–5]. Edwards *et al.* [3] applied simulations and exact enumeration to investigate this scaling law for bond percolation clusters, while Debierre [4] deduced from large-scale simulations the exact fragmentation exponent: $\phi = 1.548$. Campi *et al.* [1] reported fragment size distributions that resulted from high energy nuclear collisions, which are remarkably well reproduced by a percolation model. Similar results have been obtained by analysing a supercritical Lennard-Jones fluid [5]. The connection between the fragmentation behavior and phase transitions have been recognized very early [6]. With the help of the liquid drop model for nuclei Fisher calculated the appearance of the droplets from the Gibbs free energy. Later on fragmentation data based on Molecular Dynamics simulations were fitted to these formulas for nuclear matter [7] and atomic clusters [8]. They exhibit exactly the three fragmentation regimes discussed earlier with the power-law dependence included. The latter can be traced back to the behavior of critical phenomena. Gross *et al.* [9] studied the influence of phase transitions on the fragmentation in atomic clusters on a more general thermodynamical basis. Another attempt in this direction has been carried out for the fragmentation data of H_{25}^+, which are available on an event-by-event basis [10,11]. A further possibility for the interpretation of fragmentation data is the extreme statistical limit, the maximal entropy limit. In this way Levine and coworkers predicted the shattering of high velocity impact of atomic clusters at hard surfaces [2] and the fragmentation pattern of C_{60} and the ions after high energy collisions and photoionisation [12]. The collision dynamics and fragmentation of large water clusters have

[a] e-mail: ubuck@gwdg.de

been studied by Svanberg *et al.* in extensive MD simulations [13].

Recently, one of us investigated the fragmentation statistics of large $(H_2O)_n$ and $(NH_3)_n$ clusters in the size range from $n = 100$ to 1000 based on MD simulations. The fragment size distributions are found to be well described by power laws, as are observed in percolation theory and in the Fisher model [6]. This is valid over a wide range of excitation energies which are produced by raising the temperature of the cluster. A compact analytical model was derived for the average fragment size, implying the maximum fragment size and the power law exponent of the fragment size distribution. A preliminary account of this work has been published as brief report [14]. Here we would like to present a detailed description of the methods applied and the results. In addition, we will compare the results with recent measurements of the fragmentation behaviour of water and ammonia clusters after electron bombardment in the very same size range [15]. Although the experimental results do not exhibit the complete fragmentation pattern, they can be compared with the calculation in view of the dependence of the maximum fragment size $s_{\max}$ on the size n of the starting cluster. The remarkable agreement of this property can, in turn, be used to calculate, based on the derived analytical formulas, the average fragment size $\langle s \rangle$ and the distribution of the fragments.

The paper will be organised as follows. In Section 2 examples of the cluster structure and their behaviour will be discussed. In Section 3, the detailed results of the fragmentation pattern and the analysis will be presented. The experimental results will be shown and discussed in Section 4.

2 Cluster structures

Both the H_2O and the NH_3 monomers have been assumed to be rigid. The interactions of the H_2O monomer have been modeled by the TIP4P potential of Jorgensen *et al.* [16], intensively used in the last two decades in simulations of aqueous solutions and clusters. The monomer is represented by four interaction sites, three at the nuclei (with $r_{\mathrm{OH}} = 0.9572$ Å and $\theta_{\mathrm{HOH}} = 104.52°$) and one located on the HOH bisector, 0.15 Å from the O atom towards the H atoms. Charges are carried only by the hydrogens ($q_{\mathrm{H}} = 0.52e$) and the additional site ($-2q_{\mathrm{H}}$). In addition to the Coulomb terms, the intermolecular potential consists of Lennard-Jones interactions between the oxygens only ($\sigma = 3.15358$ Å and $\varepsilon = 0.648694$ kJ/mol).

For the NH_3 molecule, the five-site potential of Impey and Klein [17] was employed, which has proven successful in simulations of liquid ammonia and of structural and spectroscopic properties of clusters [18]. The geometry is defined by the nitrogen-hydrogen distance, $r_{\mathrm{NH}} = 1.0124$ Å, and the angle between the N-H bonds and the C_3 axis of the molecule (pointing away from the H atoms), $\varphi_{\mathrm{HNC_3}} = 112.13°$. This potential features electrostatic and Lennard-Jones interactions, too. The electrostatic interaction is modeled by four interaction sites on each molecule: three sites with partial charge $q_{\mathrm{H}} = 0.462e$ located at the H-atoms, and a site with a charge $-3q_{\mathrm{H}}$ located on the C_3 axis, 0.156 Å from the N-atom towards the H-atoms. Lennard-Jones interactions are modeled only between the N-atoms by a 12-6 potential with parameters $\sigma = 3.4$ Å and $\epsilon = 1.1649$ kJ/mol.

The best suited MD integrator was found to be the Verlet algorithm (in the quaternion representation), known to have fair energy conservation properties. We have used throughout a time step of 0.2 fs, typically ensuring a relative energy conservation error of less than 10^{-4}.

For both molecular species, clusters of sizes $n = 100$–1000 have been prepared, with an increment of 100 molecules. Their geometrical equilibrium structures have been determined by simulated annealing. For the temperature, the usual definition, as mean kinetic energy per degree of freedom, was adopted. The initial configuration of each cluster was chosen to be a sphere cut from the respective crystal. For water we considered cubic ice, which is a metastable form occurring under normal pressure conditions below 200 K. It has fcc structure, the unit cell comprises eight molecules and its dimension is 6.358 Å [19]. The solid state structure of ammonia (space group $P2_13$) was extracted from the neutron diffraction study of Reed *et al.* [20]. After an initial uniform heating at 150 K (by assigning random, properly normalized velocities to all molecules), the crystal spheres have been cooled off for 100 ps, by removing 1% of the kinetic energy at each time step. For each cluster size, 10 relaxed configurations have been prepared starting from different initial velocity patterns. The energetically lowest lying was adopted as equilibrium structure and was further used in the fragmentation calculations.

The equilibrium configurations for the water clusters with $n = 100$, 500, and 1000 are depicted in Figure 1, and the corresponding configurations of the ammonia clusters are presented in Figure 2. We note that for the water clusters the weight of the amorphous outer shell decreases with increasing cluster size and the original crystalline arrangement is preserved to a concomitantly increasing extent.

The binding energies of the equilibrium cluster structures are characterized by almost constant values per molecule: $E_{\mathrm{bind}}/n = 46.55$ kJ/mol for water and $E_{\mathrm{bind}}/n = 29.51$ kJ/mol for ammonia. The quantities characterizing the geometrical structures are found to obey power-laws. For example, the maximal extension and the gyration radius of the H_2O clusters can be very accurately fitted by $R_{\max} = 2.762n^{0.3986}$ and $R_{\mathrm{gyr}} = 1.245n^{0.3595}$, respectively, with exponents quite close to the intuitive value of 1/3. The ammonia clusters exhibit a similar behavior.

The water clusters show a quite interesting behaviour in the investigated size range. The surface appears to be definitely amorphous. In order to characterize the extent to which the cluster structures preserve the initial crystalline arrangement, we defined the "crystallinity" parameter:

$$\chi = \frac{\sum_i^{\text{all atoms}} \langle \mathbf{r}_i \cdot \mathbf{r}_i^{\mathrm{c}} \rangle}{\sum_i^{\text{all atoms}} \langle \mathbf{r}_i^{\mathrm{c}} \cdot \mathbf{r}_i^{\mathrm{c}} \rangle}, \tag{1}$$

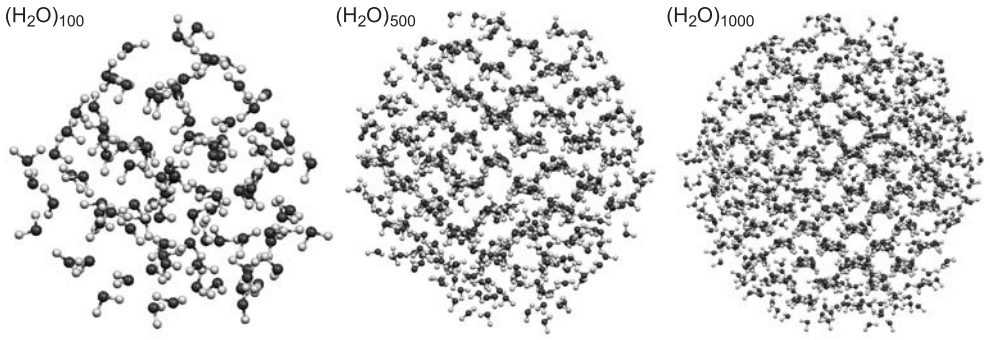

Fig. 1. Geometrical equilibrium structures of representative $(H_2O)_n$ clusters.

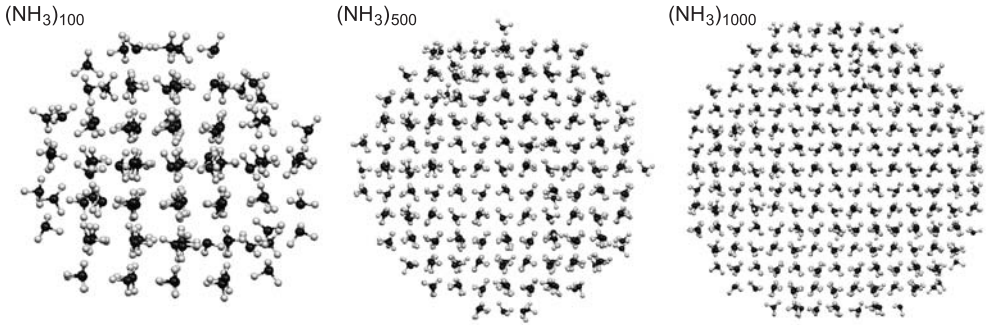

Fig. 2. Geometrical equilibrium structures of representative $(NH_3)_n$ clusters.

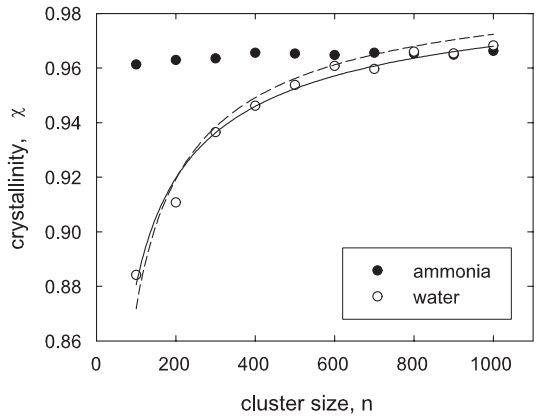

Fig. 3. Crystallinity χ of the $(H_2O)_n$ and $(NH_3)_n$ clusters as defined in (1). The solid line is the best fit, while the dashed line represents the $n^{-2/3}$ fit.

as normalized projection of the final atomic positions, $\mathbf{r}_i$, onto the corresponding crystalline positions, $\mathbf{r}_i^c$. The calculated crystallinity values, as are depicted in Figure 3 for H_2O by open circles, suggest the cluster size dependence: $\chi = 1 - an^{-b}$ and the regression yields $a = 1.662$ and $b = 0.572$ for H_2O. Nonetheless, a quite reasonable fit results also by using the single parameter functional with $b = 2/3$ (intuitively, the crystallinity should increase towards 1 by a quantity inverse proportional to the surface-to-volume ratio of the cluster considered spherical and with the outer shell molecules primarily responsible for the distortion). The optimized parameter for H_2O in this case is $a = 2.761$. This is a remarkable result, since this relation has been extensively used for the size determination of microcrystallites or aerosol particles by measuring independently the volume and the surface [21]. The reason for this behaviour, which is also confirmed experimentally [22], is the inconsistency of the small, spherical surface with a 2D periodic structure. It forces the bonds to get distorted. If we perform the same analysis for ammonia clusters, as is shown by the black circles in Figure 3, the result is completely different. Apparently, the surface preserves the crystallinity by keeping the crystal planes at the expense of the increase of the surface area. This is nicely observed in Figure 2.

3 Simulation of the fragmentation process

The excitation mechanism preceding the fragmentation was chosen to heat the cluster uniformly. In this way we kept the mechanism as general as possible. Actually, all molecules have been assigned random initial translational and rotational velocities, normalized in accordance to each chosen temperature (defined as the mean kinetic energy per degree of freedom). Rather then specifying the total excitation energy, we will refer in what follows to the corresponding temperature. The excitation temperatures considered for H_2O have been $T = 1500, 1650, 2000, 2500$, and 3000 K, corresponding to total excitation energies between $0.8E_{\rm bind}$ and $1.6E_{\rm bind}$ ($E_{\rm bind}$ being the total binding energy of the cluster). Since below 1500 K the clusters persist statistically unfragmented, lower temperatures have

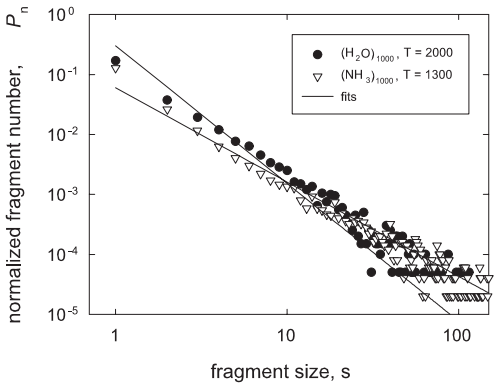

Fig. 4. Simulated normalized fragment size distributions and profiles $P_n(s)$ resulted from the model (3–8) for the $(H_2O)_{1000}$ cluster heated at 2000 K and for the cluster $(NH_3)_{1000}$ heated at 1300 K, respectively.

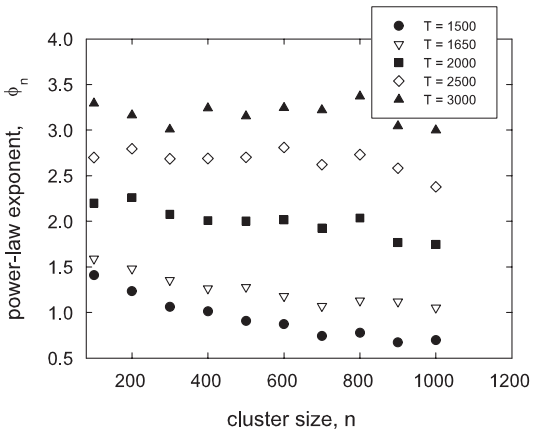

Fig. 5. Dependence of the power law exponents ϕ_n of the fragment size distributions on the size of the initial water clusters for different temperatures.

not been considered. For similar reasons, the NH_3 clusters have been heated at $T = 1000$, 1100, 1200, 1300, and 1500 K, corresponding to total excitation energies between $0.8E_{\rm bind}$ and $1.3E_{\rm bind}$.

Each fragmentation trajectory was propagated at constant energy until the overall extent of the fragment cloud exceeded four times the initial extent, for up to 10 ps. At the end of the trajectory, the individual fragments have been identified by a recursive labeling algorithm, which basically extends the fragments gradually by molecules, which lie within a cutoff distance. The cutoff was defined by the minimum intermolecular distance in the relaxed cluster increased by 1 Å.

In order to achieve reliable statistics, an ensemble of 50 identical clusters was fragmented for each molecular species, excitation temperature and cluster size, and the resulted profiles have been averaged. Thus, the fragment size distribution $P_n(s)$ specifies the average number of fragments of each particular size s resulted from the cluster of size n, normalized such that $\sum_s sP_n(s) = 1$. This normalization practically means that $P_n(s)$ is normalized to both the cluster size n and the size of the ensemble.

Several revealing findings may be obtained from the calculation of the fragmentation profiles for the relaxed water and ammonia clusters as function of the temperature and the cluster size. Typical results are presented in Figure 2 of reference [14]. Qualitatively, they all look quite similar so that we only show one selected example for $(H_2O)_{1000}$ and $(NH_3)_{1000}$ in Figure 4. In a quantitative way, they depend both on the temperature and on the system studied. We also note that the optimized cluster structures were used in the analysis, since amorphous and crystalline clusters gave different profiles for the same size. The results can be summarized as follows:

(1) the distributions are dominated by small fragments. The general fall off goes over four orders of magnitude;
(2) all profiles are affected by quite significant statistical fluctuations in the region of larger fragment sizes;
(3) the profiles for larger excitation temperatures imply relatively more small fragments, reflecting the fact that larger energy inputs split the original cluster into smaller fragments;
(4) though broadened by statistical fluctuations in the region of larger and inherently less frequent fragment sizes, the profiles for both molecular species clearly exhibit a power-law behavior of the kind

$$P_n(s) \sim s^{-\phi_n}, \tag{2}$$

similarly to the thoroughly investigated percolation clusters [4] or the results of the Fisher model [6–8];
(5) the most important quantitative difference between the H_2O and NH_3 clusters predicted by the calculations regards the very excitation temperature range in which the power-law behavior is present — the temperatures applying to H_2O are larger roughly by a factor of 2, reflecting, as discussed previously, the larger corresponding binding energies $E_{\rm bind}/n$.

The fragmentation of the H_2O clusters around and above $T = 2500$ K ($E_{\rm exc} \geq 1.3E_{\rm bind}$) seems to be somewhat better described by stretched exponentials. In the case of NH_3, the transition to stretched exponentials occurs at $T = 1500$ (*i.e.* again for $E_{\rm exc} \geq 1.3E_{\rm bind}$).

The features of the fragmentation profiles are similar to those found in the distributions obtained by Svanberg *et al.* [13] from simulations of the collision dynamics of large water clusters.

The plots of the power law exponent, ϕ_n, as shown for the water clusters in Figure 5, are different for the different excitation temperatures and indicate also a weak dependence on the cluster size. Similar results have been obtained for ammonia clusters [14]. The cluster size dependence can again be conveniently described by a power law of the type

$$\phi_n = bn^{-c}. \tag{3}$$

The parameters b and c depend, in turn, on the temperatures by

$$b(T) = b_0 + b_1 \exp(-b_2 T), \tag{4}$$

$$c(T) = c_1 \ \exp(-c_2 T). \tag{5}$$

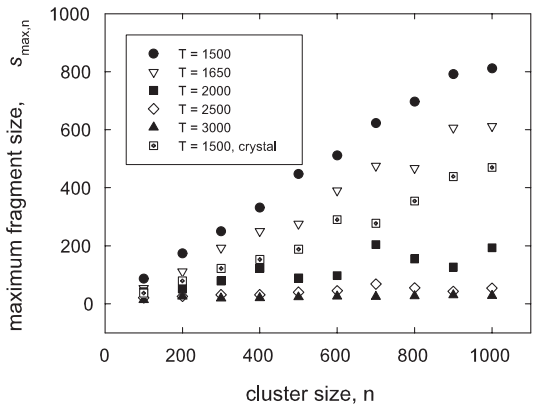

Fig. 6. Maximum fragment size $s_{\max,n}$ as a function of the size n of the initial $(H_2O)_n$ cluster.

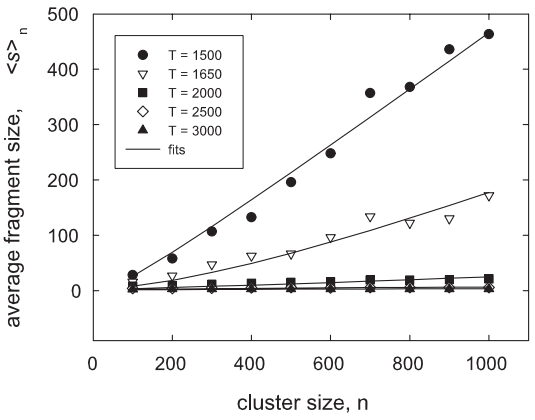

Fig. 7. Average fragment size $\langle s\rangle_n$ as a function of the size of the initial H_2O cluster from MD simulations (symbols) and calculations based on (8).

There are two properties of the fragmentation distributions with less detailed information. These are the maximum fragment size $s_{\max,n}$ and the average fragment size $\langle s\rangle_n$. The calculated distributions of maximum fragment sizes $s_{\max,n}$ for the water clusters are plotted in Figure 6. The plots are expected to be delimited by the first bisector, $s_{\max,n} = n$, corresponding to the limiting case $T = 0$ (where no fragmentation takes place), and the horizontal line $s_{\max,n} = 1$, corresponding to $T \to \infty$ (when all clusters are completely fragmented down to monomers). The results are found to vary linearly with the cluster size and the slopes decrease with increasing temperature. Thus they can be represented by:

$$s_{\max,n} = 1 + a(n-1). \tag{6}$$

The values obtained by regression for the parameter a suggest that its temperature dependence is a simple exponential decay,

$$a(T) = a_1 \exp(-a_2 T). \tag{7}$$

The temperature fits yield $a_1 = 33.5827$ and $a_2 = 2.4472\times 10^{-3}$ K^{-1} for the water clusters, while for the ammonia clusters we get $a_1 = 3298.27$ and $a_2 = 7.8352 \times 10^{-3}$ K^{-1}.

The cluster size dependences of the average fragment size $\langle s\rangle_n$ for the various excitation temperatures are shown in Figure 7 for the H_2O clusters. Absolutely similar dependences are obtained for the NH_3 clusters [14]. The profiles are again delimited by the lines $\langle s\rangle_n = n$ and $\langle s\rangle_n = 1$ for the same reasons as in the case of $s_{\max,n}$. By definition, the average fragment size is given by:

$$\langle s\rangle_n = \frac{\sum_{s=1}^{s_{\max,n}} s^2 P_n(s)}{\sum_{s=1}^{s_{\max,n}} s P_n(s)}.$$

An approximate analytic expression may be readily obtained by replacing the sums by integrals ($\sum_{s=1}^{s_{\max,n}} \cdots \simeq \int_1^{s_{\max,n}} \cdots \mathrm{d}s$) and by using the power-law distribution (2):

$$\langle s\rangle_n = \frac{2-\phi_n}{3-\phi_n} \frac{s_{\max,n}^{3-\phi_n} - 1}{s_{\max,n}^{2-\phi_n} - 1}. \tag{8}$$

For known values of the power law exponent ϕ_n and of the maximum fragment size $s_{\max,n}$, this relation should provide consistently an estimate of the average fragment size $\langle s\rangle_n$. For practical applications, however, this is hardly the case. Whereas measurements are likely to provide $s_{\max,n}$ and perhaps $\langle s\rangle_n$, the fragment size distribution itself is more difficult to obtain. Instead, relation (8) can be used in conjunction with the n-dependence of $s_{\max,n}$ (6) to deconvolute the fragmentation information obtaining ϕ_n, and thus to predict the fragment size distribution.

Relation (8) with the input from (6) and (3) define explicitly the average fragment size $\langle s\rangle_n$ as a function of the cluster size n, with adjustable parameters b and c. In fact, we used this set of equations to simultaneously fit the cluster size dependences of the average fragment size and of the power law exponents. The optimized values of the parameters b and c for the various temperatures following the exponential dependences of (4) and (5) yields for the H_2O clusters: $b_0 = 3.1976$, $b_1 = 494.22$, $b_2 = 3.1308 \times 10^{-3}$ K^{-1}, $c_1 = 9.3408$, and $c_2 = 2.2969 \times 10^{-3}$ K^{-1}. The values for the NH_3 clusters are: $b_0 = 3.1895$, $b_1 = 233574$, $b_2 = 8.9334 \times 10^{-3}$ K^{-1}, $c_1 = 15.3306$, and $c_2 = 3.4363 \times 10^{-3}$ K^{-1}. The predictions for the average fragment size $\langle s\rangle_n$ are also shown in Figure 7.

The usefulness of model (8) can be appreciated from Figure 4, where, along with the simulated fragment size distributions for the cluster $(H_2O)_{1000}$ heated at 2000 K and for the cluster $(NH_3)_{1000}$ heated at 1300 K, respectively, there have been plotted the corresponding curves resulted by using model (8) with (6) and (3), together with the temperature fits of the implied parameters $a(T)$, $b(T)$, and $c(T)$ according to (7), (4), and (5).

Some discrepancies between model and observations occur in the low temperature region due to the inherently more significant fluctuations. To overcome these, much larger ensembles of observations are needed. Some discrepancies at large excitation energies (beyond $1.3E_{\mathrm{bind}}$) are caused by the gradual transition of the profiles into stretched exponentials. However, the fair overall agreement justifies the applicability of model (8) for predicting

exponents of the fragment size distribution from maximum and average fragment sizes.

4 Experimental results and discussion

Experimental results on the fragmentation of neutral clusters are still quite rare because of the ubiquitous problem of fragmentation when the clusters are ionised for the detection process. This is a special problem for weakly bound systems, since the ionic potential curves are usually much stronger bound and shifted to smaller distances. Thus when going from the neutral to the ionic configuration, highly excited vibrational states are reached, which lead subsequently to severe fragmentation. This fact is much less dramatic for systems with delocalised electrons, since in such cases the ground state of the ionic system can be reached provided the ionisation energy can be adjusted close to the threshold region. Typical examples are the photoionisation of aromatic molecules or metals. Recently, we found an interesting way to apply such a procedure also to weakly bound systems like rare gases or hydrogen bonded systems. We dope these clusters with a single sodium atom and apply photoionisation for the detection [15,23].

The experiments have been carried out in a molecular beam machine which has been described in detail in [23]. The clusters are generated by an adiabatic expansion through nozzles of conical shape. By varying the pressure and the temperature, the size distribution can be shifted to nearly every desired size. New scaling laws which relate the source conditions to the actual sizes of water and ammonia clusters are given in [15].

Typical parameters are a conical nozzle with a diameter of 79 μm, an opening angle of $2\alpha = 25.0°$, and a length of $l = 4$ mm as well as temperatures between 412 and 480 K and pressures between 3.5 and 18.0 bar. The clusters are detected in a reflectron time-of-flight mass spectrometer. The design of the ion source allows us to simultaneously use laser photons and electrons for ionisation. The sodium doped water clusters are detected close to the threshold for ionisation at 3.2 eV which can easily be reached by dye lasers. For the ammonia clusters we used an alternative approach. Here also the (1+1)-resonance enhanced two photon ionisation (REMPI) process *via* the $\tilde{A}\,^1A_2''$ $v = 6$ state at 193 nm worked up to cluster sizes of more than $n = 3000$. Apparently, the lifetime of this state in the cluster environment is long enough to be reached by the second photon in the nanosecond regime. The results are corrected for possible multi-photon processes [24]. In addition, there is a certain amount of excess energy in the system which, however, does not lead to the evaporation of more than 25 molecules. This result is within the usual errors of the size determination in this type of experiments.

Having established a reliable method to measure the size distributions of the molecular clusters by photoionisation, we can compare them with the results obtained by the ionisation with electron impact under the same experimental conditions. The result of such a measurement

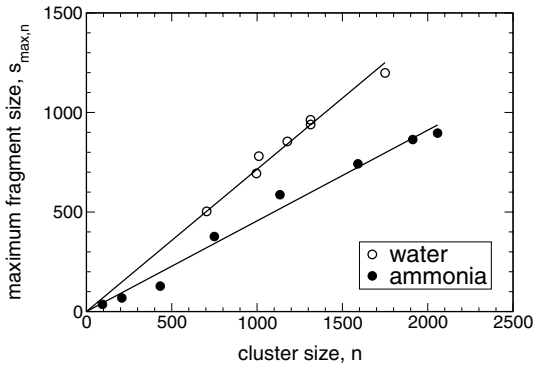

Fig. 8. Measured maximum fragment size as function of the initial cluster size for water and ammonia clusters. The fragmentation is caused by electron impact at 550 eV and 243 eV, respectively, close to the maximum of the distribution.

gives directly the maximal fragment size. In Figure 8 these maximal fragment sizes are depicted for $(NH_3)_n$ clusters obtained at electrons energies of 243 eV and $(H_2O)_n$ clusters at 550 eV. The different electron energies have been chosen to be close to the maximum of the fragmentation probabilities of the respective system. The results of electron impact are corrected for doubly ionised clusters [15]. In both cases we find a linear dependence on the cluster size n, but the absolute numbers are about a factor of two smaller for ammonia.

This behaviour is exactly predicted in the present calculations in Figure 6 and the relation (6). Even if we take into account that in the experiment log-normal distributions are measured, the conclusions are the same, since the convolution of a log-normal distribution with a linear behaviour results in a log-normal distribution. What, in fact, is plotted in Figure 6 are the maxima of these distributions. Thus, we are now able to derive from the slope of the measured curve the temperature which leads to the same fragmentation pattern for $s_{\max,n}$, namely $T = 1573$ K for water and $T = 1134$ K for ammonia clusters. Given these values, we can go one step further and calculate the fragment size distribution $P_n(s)$ according to (2) and the average fragment size $\langle s \rangle_n$ by applying (8). They will look very similar to the curves displayed in Figure 4. We note that the experimental result of a lower excitation temperature for ammonia clusters is in line with all the calculations and is certainly a reflection of the lower binding energy of this cluster. In this way the combination of MD simulations using realistic interaction potentials, the analysis based on percolation theory and restricted, but reliable experimental data lead to a complete description of the fragmentation process. We note that also in the evaporation limit a linear behavior of the fragment size as function of the original size should result. We found for the electron impact ionisation of large Ar_n clusters at 70 eV such a behavior [25]. But in contrast to the present result, the number of evaporated particles was much smaller, in the range of tens compared to hundreds in the power-law regime. The direct experimental proof, the measurement

of the product size distribution, was not carried out in the present experiment.

What is interesting to note is the fact that interaction of electrons in the energy range of a couple of hundred electron volts can be described by a fragmentation theory that is simply based on heating the cluster. The explanation of these measurements given in reference [15] was essentially based on the energy dependence of the yield of the ejected particles which is proportional to the stopping power. It followed precisely what is known from the sputtering of solid material. The sputtering of these weakly bound insulator materials is dominated by electronic interactions and consists of three separate processes. First, the incoming particle interacts with the target and generates electronic excitations and ionisations along the track. Second, these excitations deposit energy into the solid as a result of non-radiative relaxations which appear as vibrational excitation of the target molecules. This energy has to be transported to the surface where, finally, the particles evaporate. Thus the yield is always proportional to the stopping power ($\mathrm{d}E/\mathrm{d}s$). The absolute values of the yield, however, are two orders of magnitude larger for clusters than in the case of the solids. This is explained by a simple model based on the fast distribution of heat after the excitation of a small finite sample. The spread of this energy can be described by the heat equation of a temperature field $T(t, r)$, which is a function of the time t and the spatial coordinate r. After 20 ps the heat has spread over 10 nm. Obviously the cluster cannot accommodate the excitation energy and nearly evaporates completely. We note that already in this part of our previous explanation a temperature field had to be invoked in order to explain the data. Finally we note that we have also observed other cases where the typical ingredients of the present model, the power law of the fragment size distribution, is not observed. After the vibrational excitation of the OH stretch mode in large water clusters, the fragment distribution did not show a decreasing power law, but a maximum of the intensity around $s = 6$ [26]. In this case, the dynamical process of the coupling of the intramolecular vibrations to the dissociative intermolecular motion can apparently not be described by simply heating the system.

This work was supported by the Deutsche Forschungsgemeinschaft and the Graduiertenkolleg 782. We thank Dr. S. Schütte and Dr. C. Bobbert for measuring the data of Figure 8.

References

1. X. Campi, H. Krivine, N. Sator, E. Plagnol, Eur. Phys. J. D **11**, 233 (2000)
2. T. Raz, U. Even, R.D. Levine, J. Chem. Phys. **103**, 5394 (1995)
3. B.F. Edwards, M.F. Gyure, M. Ferer, Phys. Rev. A **46**, 6252 (1992)
4. J.-M. Debierre, Phys. Rev. Lett. **78**, 3145 (1997)
5. X. Campi, H. Krivine, N. Sator, Physica A **296**, 24 (2001)
6. M.E. Fisher, Rep. Prog. Phys. **30**, 615 (1967)
7. M. Belkacem, V. Latora, A. Bonsera, Phys. Rev. C **52**, 271 (1995)
8. V.N. Kondratyev, H.O. Lutz, Z. Phys. D **40**, 210 (1997)
9. D.H.E. Gross, M.E. Madjet, O. Schapiro, Z. Phys. D **39**, 75 (1997)
10. B. Farizon, M. Farizon, M.J. Gaillard, F. Gobet, G. Guillermier, M. Carré, J.P. Buchet, P. Scheier, T.D. Märk, Phys. Rev. Lett. **81**, 4108 (1998)
11. B. Farizon, M. Farizon, M.J. Gaillard, F. Gobet, M. Carré, J.P. Buchet, P. Scheier, T.D. Märk, Eur. Phys. Lett. **5**, 5 (1999)
12. E.E.B. Campbell, T. Raz, R.D. Levine, Chem. Phys. Lett. **253**, 261 (1996)
13. M. Svanberg, L. Ming, N. Markovic, J.B.C. Petterson, J. Chem. Phys. **108**, 5888 (1998)
14. T.A. Beu, Phys. Rev. A **67**, 045201 (2003)
15. C. Bobbert, S. Schütte, C. Steinbach, U. Buck, Eur. Phys. J. D **19**, 183 (2002)
16. W.L. Jorgensen, J. Chandrasekhar, J.D. Madura, R.W. Impey, M.L. Klein, J. Chem. Phys. **79**, 926 (1983)
17. R.W. Impey, M.L. Klein, Chem. Phys. Lett. **104**, 579 (1984)
18. T.A. Beu, C. Steinbach, U. Buck, J. Chem. Phys. **117**, 3149 (2002)
19. L.G. Dowell, A.P. Rinfret, Nature **188**, 1144 (1960)
20. J.W. Reed, P.M. Harris, J. Chem. Phys. **35**, 1730 (1961)
21. J.P. Devlin, J. Sadlej, V. Buch, J. Phys. Chem. A **105**, 974 (2001)
22. J.P. Devlin, C. Joyce, V. Buch, J. Phys. Chem. A **104**, 1974 (2000)
23. S. Schütte, U. Buck, Int. J. Mass Spec. **220**, 183 (2002)
24. S. Schütte, U. Buck, Appl. Phys. A **69**, S209 (1999)
25. P. Lohbrandt, R. Galonska, H.-J. Kim, M. Schmidt, C. Lauenstein, U. Buck, in *Atomic and Molecular Beams* (Springer, Berlin, 2001), p. 623
26. P. Andersson, C. Steinbach, U. Buck, Eur. Phys. J. D **24**, 53 (2003)